Geosci. Model Dev. Discuss., 7, 5049–5085, 2014
www.geosci-model-dev-discuss.net/7/5049/2014/
doi:10.5194/gmdd-7-5049-2014

Geoscientific Model Development Discussions
Open Access

Assessing the nonlinear response of fine particles to precursor emissions: development and application of an Extended Response Surface Modeling technique (ERSM v1.0)

B. Zhao[1], S. X. Wang[1,2], K. Fu[1], J. Xing[3], J. S. Fu[4], C. Jang[3], Y. Zhu[5], X. Y. Dong[4], Y. Gao[4,6], W. J. Wu[1], and J. M. Hao[1,2]

[1]State Key Joint Laboratory of Environment Simulation and Pollution Control, School of Environment, Tsinghua University, Beijing 100084, China
[2]State Environmental Protection Key Laboratory of Sources and Control of Air Pollution Complex, Beijing 100084, China
[3]US Environmental Protection Agency, Research Triangle Park, North Carolina 27711, USA
[4]Department of Civil and Environmental Engineering, University of Tennessee, Knoxville, Tennessee 37996, USA
[5]School of Environmental Science and Engineering, South China University of Technology, Guangzhou 510006, China

[6]Atmospheric Science and Global Change Division, Pacific Northwest National Laboratory, Richland, Washington, 99352, USA

Received: 13 July 2014 – Accepted: 16 July 2014 – Published: 5 August 2014

Correspondence to: S. X. Wang (shxwang@tsinghua.edu.cn)

Published by Copernicus Publications on behalf of the European Geosciences Union.

GMDD
7, 5049–5085, 2014

Abstract

An innovative Extended Response Surface Modeling technique (ERSM v1.0) is developed to characterize the nonlinear response of fine particles ($PM_{2.5}$) to large and simultaneous changes of multiple precursor emissions from multiple regions and sectors. The ERSM technique is developed starting from the conventional Response Surface Modeling (RSM) technique; it first quantifies the relationship between $PM_{2.5}$ concentrations and precursor emissions in a single region with the conventional RSM technique, and then assesses the effects of inter-regional transport of $PM_{2.5}$ and its precursors on $PM_{2.5}$ concentrations in the target region. We apply this novel technique with a widely used regional air quality model over the Yangtze River Delta (YRD) region of China, and evaluate the response of $PM_{2.5}$ and its inorganic components to the emissions of 36 pollutant-region-sector combinations. The predicted $PM_{2.5}$ concentrations agree well with independent air quality model simulations; the correlation coefficients are larger than 0.98 and 0.99, and the mean normalized errors are less than 1 and 2 % for January and August, respectively. It is also demonstrated that the ERSM technique could reproduce fairly well the response of $PM_{2.5}$ to continuous changes of precursor emission levels between zero and 150 %. Employing this new technique, we identify the major sources contributing to $PM_{2.5}$ and its inorganic components in the YRD region. The nonlinearity in the response of $PM_{2.5}$ to emission changes is characterized and the underlying chemical processes are illustrated.

1 Introduction

Fine particles (i.e., particulate matter less than or equal to 2.5 µm ($PM_{2.5}$)) worsen the visibility (Zhang et al., 2012), pose serious health risks (Nel, 2005) and affect the Earth's climate significantly (Stocker et al., 2013). For developing countries like China and India, the attainment of stringent ambient $PM_{2.5}$ standards requires large reductions of both primary particles and gaseous precursors (Wang and Hao, 2012).

GMDD
7, 5049–5085, 2014

Cost-effective control policies need to consider the impact of emission reductions of multiple pollutants from multiple regions and sectors, and over a wide range of stringency levels. Therefore, it is strategically important to assess the response of $PM_{2.5}$ to its precursor emissions from multiple sources, which is typically nonlinear owing to complex chemical mechanisms.

Air quality models are the only viable tools for evaluating the response of atmospheric concentrations to different control measures (Hakami et al., 2003). The most widely used technique to evaluate these responses is sensitivity analysis, i.e., the computation of derivatives of modeled concentrations with respect to emission rates. "Brute force" method (Russell et al., 1995; Y. Zhang et al., 2009; Zhao et al., 2013c; Dong et al., 2014), the most frequently used method for sensitivity analysis, involves one-at-a-time variable perturbation and repeated solution of the model. It is straightforward but becomes inefficient for decision-making when cost-effective emission controls need to optimize over various pollutants from multiple sources. A number of mathematic techniques embedded in air quality models have been developed to simultaneously calculate the sensitivities of the modeled concentrations to multiple variables, including the Green Function Method (GFM) and its variations (Hwang et al., 1978), Automatic DIfferentiation in FORtran (ADIFOR, Carmichael et al., 1997), Direct Method (Dickerson et al., 1982), Decoupled Direct Method (DDM, Yang et al., 1997), and Adjoint Sensitivity Analysis (Sandu et al., 2005; Hakami et al., 2006). These methods are used for the calculation of first-order sensitivities, and are therefore not applicable for large emission changes since the nonlinearity in atmospheric responses is not captured by first-order sensitivities. Improved techniques incorporating second or higher-order sensitivity analysis, e.g., High-order Decoupled Direct Method (HDDM, Hakami et al., 2003), and Discrete Second Order Adjoints (Sandu and Zhang, 2008), are capable of capturing the nonlinearity for a perturbation of the emissions of the base case. But as methods for local sensitivity analysis, they are theoretically not reliable for predicting the response of atmospheric concentrations to considerably large (e.g., > 50–60 %) emission reductions (Yarwood et al., 2013), which are nevertheless very common in

GMDD
7, 5049–5085, 2014

air quality policy-making of developing countries like China (Zhao et al., 2013b; Wang et al., 2014). Recent studies (Yarwood et al., 2013; Simon et al., 2013) tried to run HDDM at several emission levels and use piecewise function to predict the atmospheric concentrations over a large emission range, but this modified method is only suitable for 2–3 variables. More importantly, this group of method could hardly predict the response of atmospheric concentrations when multiple (> 3) variables of precursor emissions change simultaneously.

Another group of methods involves building the relationship between the modeled concentrations and emission rates using statistical techniques. This type of method is applicable for various air quality models regardless of the chemical mechanisms, is user-friendly for decision-makers, and is particularly suitable for assessing the atmospheric response to large emission changes. Milford et al. (1989) and Fu et al. (2006) simulated the ozone concentrations for a number of non-methane volatile organic compound (NMVOC) and NO_X reduction combinations, and derived a set of "EKMA-like" (EKMA, Empirical Kinetics Modeling Approach) control isopleths, but this method is only suitable for 2–3 variables. Some other studies (Heyes et al., 1996; Wang and Milford, 2001; Amann et al., 2007; Carnevale et al., 2009) empirically established analytic equations for the relationship between atmospheric concentrations and emission rates, and determined the parameters based on relatively small numbers of model simulations. However, Xing (2011) indicated that the nonlinearity in atmospheric responses could not be captured in metropolitan regions unless fourth or higher order equations were used, which restricted the feasibility and accuracy of analytic equations. The Response Surface Modeling (RSM) technique (denoted by "conventional RSM" technique in the following text to distinguish from the ERSM technique developed in this study), has been developed by using advanced statistical techniques to characterize the relationship between model outputs and inputs in a highly economical manner. It has recently been successfully applied for a series of O_3 and $PM_{2.5}$ related researches or policy-making in United States (US Environmental Protection Agency, 2006a, b) and China (Xing et al., 2011; Wang et al., 2011). But a major limitation for the conventional

GMDD
7, 5049–5085, 2014

RSM technique is that the number of model scenarios required to build the response surface depends on the variable number via an equation of fourth or higher order. Therefore, hundreds of thousands of model scenarios are required to build the response surface for 10–15 or more variables, which is computationally impossible for most three-dimensional air quality models. When considering the emissions of multiple pollutants from multiple sectors in multiple regions, assessing the nonlinear response of $PM_{2.5}$ to emission changes presents a big challenge.

In response to this challenge, we developed a novel Extended Response Surface Modeling technique (ERSM v1.0) in this study. Compared with the previous methods reviewed above, this technique could characterize the nonlinear response of $PM_{2.5}$ and its chemical components to large and simultaneous changes of multiple precursor emissions from multiple regions and sectors with a reasonable number of model scenarios. This technique is applied with the Community Multi-scale Air Quality (CMAQ) model to evaluate the response of $PM_{2.5}$ and its inorganic components to precursor emissions over the Yangtze River Delta (YRD) region, one of the largest city-clusters in China. The major sources contributing to $PM_{2.5}$ and its inorganic components in the YRD are identified and the nonlinearity in the response of $PM_{2.5}$ to emission changes is characterized.

2 Methodology

2.1 Development of the ERSM technique

The ERSM technique is developed starting from the conventional RSM technique; the latter characterizes the relationships between a response variable (e.g., $PM_{2.5}$ concentration) and a set of control variables (i.e., emissions of particular precursors from particular sources) following the procedures described in our previous paper (Xing et al., 2011). A number of emission control scenarios are generated with the Latin Hypercube Sample (LHS) method (Iman et al., 1980), a widely-used sampling method

GMDD
7, 5049–5085, 2014

which ensures that the ensemble of random samples is representative of actual variability. Then the $PM_{2.5}$ concentration for each emission scenario is calculated with a regional air quality model, and finally the RSM prediction system is developed using a MPerK (MATLAB Parametric Empirical Kriging) program (Santner et al., 2003) based on Maximum Likelihood Estimation Experimental Best Linear Unbiased Predictors (MLE-EBLUPs).

The ERSM technique first quantifies the relationship between $PM_{2.5}$ concentrations and its precursor emissions from a single region with the conventional RSM technique, and then assesses the effects of inter-regional transport of $PM_{2.5}$ and its precursors on $PM_{2.5}$ concentration in the target region. In order to quantify the interaction among regions, we make a key assumption that the emissions in the source region affect $PM_{2.5}$ concentrations in the target region through two major processes: (1) the inter-regional transport of gaseous precursors enhancing the chemical formation of $PM_{2.5}$ in the target region; (2) the direct transport of $PM_{2.5}$ from the source region to the target region. We quantify the contribution of these two processes to the interactions between any two regions, and assess the inter-regional influences among multiple regions by integrating the contributions of each process. Finally, a particular algorithm was implemented to improve the accuracy of the response surface when the emissions from multiple regions experience quite large reductions simultaneously. A detailed description of the ERSM technique is given below.

$PM_{2.5}$ concentrations are linearly dependent on primary $PM_{2.5}$ emissions, therefore we predict the changes of $PM_{2.5}$ concentrations owing to the changes of primary $PM_{2.5}$ emissions by simply interpolating between the base case and a sensitivity scenario where one control variable of primary $PM_{2.5}$ is disturbed and the other variables stay constant.

We will focus on the response of $PM_{2.5}$ and its chemical species to the emissions of gaseous precursors in the following texts. To facilitate the explanation, we assume a simplified but general case which involves three regions, defined as A, B, and C, and three control variables in each region, i.e., NO_X emissions of Sector 1, NO_X emissions

GMDD
7, 5049–5085, 2014

of Sector 2, and total NH_3 emissions. The response variable is $PM_{2.5}$ concentration in the urban area of Region A. Although the technique is illustrated for this simplified case, it is also applicable for different response variable (e.g., NO_3^-, SO_4^{2-}, and NH_4^+), and different numbers of regions/pollutants/sectors.

The emission control scenarios required to build the response surface include: (1) the base case; (2) *N* scenarios generated by applying the LHS method for the control variables in each single region; and (3) M scenarios generated by applying the LHS method for the total emissions of gaseous precursors (NO_X and NH_3 for this case) in all regions. The scenario numbers *N* and *M* are determined in order that they are sufficient to construct the relationship between the response variable and randomly changing control variables. The response surface for 2 and 3 variables could be built with 30 and 50 scenarios, respectively (Xing et al., 2011; Wang et al., 2011); therefore, $N = 50$, and $M = 30$. For the simplified case, the required scenario number is therefore 1 (the base case) + 50 (scenarios for each single region) · 3 (number of regions) + 30 (scenarios for the total precursor emissions in all regions) = 181.

Employing conventional RSM technique, we build the response surface of $PM_{2.5}$ concentration in Region A to the concentrations of precursors in Region A using the base case and the 50 scenarios where the variables in Region A change randomly but those in other regions remain constant:

$$\left[PM_{2.5}\right]_A = \left[PM_{2.5}\right]_{A0} + RSM_{A\to A}^{PM_{2.5}}\left([NO_x]_A, \left[NH_3\right]_A\right) \quad (1)$$

where $\left[PM_{2.5}\right]_A$, $[NO_x]_A$, and $\left[NH_3\right]_A$ are the concentrations of $PM_{2.5}$, NO_X and NH_3 in Region A, respectively. $\left[PM_{2.5}\right]_{A0}$ is the $PM_{2.5}$ concentration in Region A in the base case. RSM represents the response surface we build with conventional RSM technique; the superscript ("$PM_{2.5}$" in this case) represents the response variable; the letters before and after the arrow in the subscript (both are "A" in this case) represent the source and receptor regions, respectively. Further, we develop the relationship between precursor concentrations and the changes of precursor emissions in Region A with the same 51 scenarios (we use NO_X concentration as example, and it is the same as

GMDD
7, 5049–5085, 2014

NH_3):

$$[NO_x]_{A\to A} = RSM^{NO_x}_{A\to A}\left(Emis\_NO_x\_1_A, Emis\_NO_x\_2_A, Emis\_NH_{3A}\right) \quad (2)$$

where $Emis\_NO_x\_1_A$, $Emis\_NO_x\_2_A$, and $Emis\_NH_{3A}$ are NO_X emissions of Sector 1, NO_X emissions of Sector 2, and total NH_3 emissions in Region A, respectively. $[NO_x]_{A\to A}$, representing the changes of NO_X concentration in Region A compared with the base case in response to the emission changes in the same region, is defined as

$$[NO_x]_{A\to A} = [NO_x]_A - [NO_x]_{A0} \quad (3)$$

where $[NO_x]_{A0}$ is the NO_X concentration in Region A in the base case.

Following similar procedures, the response of the concentrations of $PM_{2.5}$ and its precursors in Region A to the changes of precursor emissions in Region B (the same method applies for Region C) can be developed using the base case and the 50 scenarios where the variables in Region B change randomly but those in other regions remain constant:

$$\left[PM_{2.5}\right]_{B\to A} = RSM^{PM_{2.5}}_{B\to A}\left(Emis\_NO_x\_1_B, Emis\_NO_x\_2_B, Emis\_NH_{3B}\right) \quad (4)$$

$$[NO_x]_{B\to A} = RSM^{NO_x}_{B\to A}\left(Emis\_NO_x\_1_B, Emis\_NO_x\_2_B, Emis\_NH_{3B}\right) \quad (5)$$

$$\left[NH_3\right]_{B\to A} = RSM^{NH_3}_{B\to A}\left(Emis\_NO_x\_1_B, Emis\_NO_x\_2_B, Emis\_NH_{3B}\right) \quad (6)$$

where $\left[PM_{2.5}\right]_{B\to A}$, $[NO_x]_{B\to A}$, and $\left[NH_3\right]_{B\to A}$ are the changes of $PM_{2.5}$, NO_X, and NH_3 concentrations in Region A compared with the base case in response to the emission changes in Region B. $Emis\_NO_x\_1_B$, $Emis\_NO_x\_2_B$, and $Emis\_NH_{3B}$ are NO_X emissions of Sector 1, NO_X emissions of Sector 2, and total NH_3 emissions in Region B, respectively.

As described above, the influence of emissions in Region B on $PM_{2.5}$ concentration in Region A, as expressed by Eq. (4), can be broken down into two major processes: (1) the transport of gaseous precursors from Region B to Region A that enhances the

GMDD
7, 5049–5085, 2014

chemical formation of $PM_{2.5}$ in region A; (2) the direct transport of $PM_{2.5}$ from Region B to Region A. The effect of inter-regional transport of gaseous precursors on the precursor concentrations in Region A is quantified with Eqs. (5) and (6). We introduce another assumption that the changes of $PM_{2.5}$ concentration owing to changes of precursor concentrations in the same region (described by Eq. 1) are solely attributable to changes of local chemical formation. Therefore, the contribution of the first process to $PM_{2.5}$ concentrations in Region A is expressed as

$$\left[PM_{2.5}\_Chem\right]_{B\to A} = RSM_{A\to A}^{PM_{2.5}}\left([NO_x]_{A0} + [NO_x]_{B\to A}, [NH_3]_{A0} + [NH_3]_{B\to A}\right) \quad (7)$$

where $\left[PM_{2.5}\_Chem\right]_{B\to A}$ is the change of $PM_{2.5}$ concentration in Region A affected by the changes of precursor emissions in Region B through the inter-regional transport of precursors. The contribution of the second process to $PM_{2.5}$ concentration in Region A is then calculated by extracting the contribution of the first process (Eq. 7) from the total (Eq. 4), as expressed by Eq. (8). Then we relate it to the precursor emissions in Region B with conventional RSM technique as described by Eq. (9).

$$\left[PM_{2.5}\_Trans\right]_{B\to A} = [PM_{2.5}]_{B\to A} - \left[PM_{2.5}\_Chem\right]_{B\to A} \quad (8)$$

$$\left[PM_{2.5}\_Trans\right]_{B\to A} = RSM_{B\to A}^{PM_{2.5}\_Trans}\left(Emis\_NO_x\_1_B, Emis\_NO_x\_2_B, Emis\_NH_{3B}\right) \quad (9)$$

where $\left[PM_{2.5}\_Trans\right]_{B\to A}$ is the change of $PM_{2.5}$ concentration in Region A affected by the changes of precursor emissions in Region B through the direct transport of $PM_{2.5}$.

When the emissions of gaseous precursors change simultaneously in the three regions, the changes of $PM_{2.5}$ is expressed as an integrated effect of the changes of local precursor emissions, the inter-regional transport of precursors enhancing local chemical reactions, and the inter-regional transport of $PM_{2.5}$:

$$\begin{aligned}[PM_{2.5}]_A = {} & [PM_{2.5}]_{A0} + RSM_{A\to A}^{PM_{2.5}}([NO_x]_{A0} + [NO_x]_{A\to A} + [NO_x]_{B\to A} \\ & + [NO_x]_{C\to A}, [NH_3]_{A0} + [NH_3]_{A\to A} + [NH_3]_{B\to A} + [NH_3]_{C\to A}) \\ & + \left[PM_{2.5}\_Trans\right]_{B\to A} + \left[PM_{2.5}\_Trans\right]_{C\to A}\end{aligned} \quad (10)$$

GMDD
7, 5049–5085, 2014

Equation (10) implies an assumption that the contribution of precursor emissions in Region B to $PM_{2.5}$ concentration in Region A through direct inter-regional transport of $PM_{2.5}$ is independent of precursor emissions in other regions (except for Region B).

However, it should be noted that Eq. (1), which relates the changes of $PM_{2.5}$ concentration in Region A (equivalent to the changes of local chemical formation of $PM_{2.5}$ as discussed above) to local precursor concentrations, is established using the base case and the 50 scenarios where the variables in Region A change randomly but those in other regions remain constant. This means Eq. (1) is only applicable for the concentration range below (we use NO_X as example, the same as NH_3)

$$[NO_x]_A \geq [NO_x]_{A,min} = [NO_x]_{A0} + [NO_x]_{A\rightarrow A,min} = [NO_x]_{A0} + RSM^{NO_x}_{A\rightarrow A}(0,0,0) \quad (11)$$

Equation (10) relies on Eq. (1) but could exceed its available range, i.e., $[NO_x]_A < [NO_x]_{A,min}$, or $[NH_3]_A < [NH_3]_{A,min}$, when the precursor emissions in multiple regions are reduced considerably at the same time. In this case, we quantify the changes of $PM_{2.5}$ concentrations owing to local chemical formation through a different pathway. First, the local chemical formation of $PM_{2.5}$ can be tracked easily in widely-used three-dimensional air quality models. For example, an optional module named "process analysis" has already been implemented in CMAQ, which outputs the contribution of major physical and chemical processes to air pollutant concentrations. The chemical formation of $PM_{2.5}$ in Region A is estimated as

$$Prod\_PM_A = AERO\_PM_A + CLDS\_PM_A \quad (12)$$

where $AERO\_PM_A$ and $CLDS\_PM_A$ are the contribution of aerosol process and in-cloud process to $PM_{2.5}$ concentration in Region A, extracted from CMAQ using the module "process analysis". When the ERSM technique is applied with other air quality models, the chemical formation of $PM_{2.5}$ can be readily extracted in a similar way. In addition, the chemical formation of $PM_{2.5}$ in Region A and the resulting $PM_{2.5}$ concentrations present a linear relationship, which can be established using the base case

GMDD
7, 5049–5085, 2014

and the 50 scenarios where the variables in Region A change randomly but those in other regions remain constant:

$$[PM_{2.5}]_A = k \cdot Prod\_PM_A + b \quad (13)$$

where k and b are parameters decided through regression, and the correlation coefficient is approximately 0.99. Then we develop the relationship between the local chemical formation of $PM_{2.5}$ in Region A and local precursor concentrations using the base case and the 30 scenarios where control variables in all regions change together and the variables for the same pollutant (e.g., $Emis\_NH_{3A}$, $Emis\_NH_{3B}$, and $Emis\_NH_{3C}$) equal each other:

$$Prod\_PM_A = RSM_{A\to A}^{Prod\_PM}\left([NO_x]_A, [NH_3]_A\right) \quad (14)$$

Combining Eqs. (13) and (14), and considering the effect of inter-regional transport of $PM_{2.5}$ (calculated using Eq. 9), we derive

$$\begin{aligned}[PM_{2.5}]_A = k \cdot\ & RSM_{A\to A}^{Prod\_PM}\left([NO_x]_{A0} + [NO_x]_{A\to A} + [NO_x]_{B\to A} + [NO_x]_{C\to A}, [NH_3]_{A0}\right. \\ & \left. + [NH_3]_{A\to A} + [NH_3]_{B\to A} + [NH_3]_{C\to A}\right) + b + [PM_{2.5}\_Trans]_{B\to A} \\ & + [PM_{2.5}\_Trans]_{C\to A} \\ & \left(\text{applicable for } [NO_x]_A < [NO_x]_{A,min}, \text{ or } [NH_3]_A < [NH_3]_{A,min}\right)\end{aligned} \quad (15)$$

To assure the consistency between Eqs. (10) and (15), we introduce a "transition interval" of δ ($\delta_{NO_x} = 0.1 \cdot [NO_x]_{A0}, \delta_{NH_3} = 0.1 \cdot [NH_3]_{A0}$). Equation (10) is applied for $[NO_x]_A \geq [NO_x]_{A,min} + \delta_{NO_x}$ and $[NH_3]_A \geq [NH_3]_{A,min} + \delta_{NH_3}$, and we linearly interpolates between Eqs. (10) and (15) for the transitional range.

2.2 Case study of the YRD region

The ERSM technique was applied with CMAQ version 4.7.1 over the YRD region of China. One-way, triple nesting simulation domains are used, as shown in

GMDD
7, 5049–5085, 2014

Fig. 1. Domain 1 covers most of China and part of East Asia with a grid resolution of 36 km × 36 km; domain 2 covers the eastern China with a grid resolution of 12 km × 12 km; domain 3 covers the Yangtze River Delta region with a grid resolution of 4 km × 4 km. The Weather Research and Forecasting Model (WRF, version 3.3) was used to generate the meteorological fields. The physical and chemical options of CMAQ and WRF, the geographical projection, the vertical resolution, and the initial and boundary conditions are consistent with our previous papers (Zhao et al., 2013a, c). A high-resolution anthropogenic emission inventory for the YRD region developed by Fu et al. (2013) was used. The anthropogenic emissions for other regions in China were from Zhao et al. (2013a, c), and emissions for other Asian countries were taken from the INDEX-Binventory (Q. Zhang et al., 2009). The biogenic emissions were calculated by the Model of Emissions of Gases and Aerosols from Nature (MEGAN, Guenther et al., 2006). The simulation period is January and August in 2010, representing winter and summer, respectively. The simulated meteorological parameters, and concentrations of PM_{10}, $PM_{2.5}$, and their chemical components agree fairly well with observation data, as described in detail in the Supplement (Tables S1 and S2, Figs. S1–S3).

Domain 3 was divided into 4 regions (see Fig. 1), i.e. Shanghai, southern Jiangsu province ("Jiangsu"), northern Zhejiang province ("Zhejiang"), and other regions ("Others"). We developed two RSM/ERSM prediction systems (Table 1); the response variables for both of them are the concentrations of $PM_{2.5}$, SO_4^{2-}, and NO_3^- over the urban areas of major cities (see Fig. 1) in these four regions. The first prediction system used the conventional RSM technique and 101 emission control scenarios generated by the LHS method to map atmospheric concentrations vs. total emissions of NO_X, SO_2, NH_3, NMVOC, and $PM_{2.5}$ in Domain 3. For the second prediction system, the emissions of gaseous $PM_{2.5}$ precursors and primary $PM_{2.5}$ in each of the four regions are categorized into 6 and 3 control variables, respectively (see Table 1), resulting in 36 control variables in total. We generated 663 scenarios (see Table 1) to build the response surface, following the method to create emission scenarios for the ERSM technique (the 5th paragraph of Sect. 2.1). Note that we did not consider NMVOC emissions in the

GMDD
7, 5049–5085, 2014

second prediction system, because the contribution of NMVOC to $PM_{2.5}$ concentrations is small in the current CMAQ model, mainly due to the significant underestimation of secondary organic aerosol formation (Carlton et al., 2010).

3 Results and discussion

3.1 Validation of ERSM performance

The performance of the conventional RSM technique has been well evaluated in our previous studies (Xing et al., 2011; Wang et al., 2011). In this study we focus on the validation of the ERSM technique. Using the prediction system built with the ERSM technique, we predicted the $PM_{2.5}$ concentrations for 40 "out-of-sample" control scenarios, i.e., scenarios independent from those used to build the ERSM prediciton system, and compared with the corresponding CMAQ simulations. These 40 out-of-sample scenarios include 32 cases (case 1–32) where the control variables of gaseous precursors change but those of primary $PM_{2.5}$ stay the same as the base case, 4 cases (case 33–36) the other way around, and 4 cases (case 37–40) where control variables of gaseous precursors and primary $PM_{2.5}$ change simultaneously. These 40 scenarios include both the cases generated randomly with the LHS method, and the cases where all control variables are controlled stringently. A detailed description of the out-of-sample control scenarios is given in Table S3. Two statistical indices, the Normalized Error (NE) and Mean Normalized Error (MNE) are defined as follows:

$$\mathrm{NE} = |P_i - S_i| / S_i \tag{16}$$

$$\mathrm{MNE} = \frac{1}{\mathrm{Ns}} \sum_{i=1}^{\mathrm{Ns}} \left[|P_i - S_i| / S_i \right] \tag{17}$$

where P_i and S_i are the ERSM-predicted and CMAQ-simulated value of the ith out-of-sample scenario; Ns is the number of out-of-sample scenarios. Figure 2 compares

GMDD
7, 5049–5085, 2014

the ERSM-predicted and CMAQ-simulated $PM_{2.5}$ concentrations for the out-of-sample scenarios using scattering plots (the raw data for the scattering plots are given in Tables S4–S5). Table 2 shows the statistical results for the comparison. It can be seen that the ERSM predictions and CMAQ simulations agree well with each other. The correlation coefficients are larger than 0.98 and 0.99, and the MNEs are less than 1 % and 2 % for January and August, respectively. The maximum NEs could be as large as 6 % and 10 % in January and August, respectively, but the NEs for 95 % of all out-of-sample scenarios fall below 3.5 %. NEs exceeding 3.5 % happen only for the scenario where all control variables are reduced by 90 % (case 25). In addition, the maximum NEs for case 33–36 are all within 0.2 %, indicating a perfect linear relationship between $PM_{2.5}$ concentrations and primary $PM_{2.5}$ emissions.

We further evaluated the performance of the ERSM technique by comparing the 2-D-isopleths of $PM_{2.5}$ concentrations in response to the changes of total $NO_X/SO_2/NH_3$ emissions derived from both the conventional RSM and the ERSM technique. Figure 3–5 show the isopleths of $PM_{2.5}$ concentrations in Shanghai, Jiangsu, and Zhejiang, respectively. The *X* and *Y* axis of the figures show the "emission ratio", defined as the ratios of the changed emissions to the emissions in the base case. For example, an emission ratio of 1.5 means the emissions of a particular control variable increase by 50 % from the base case. The different colors represent different $PM_{2.5}$ concentrations. The comparison shows that the shapes of isopleths derived from both prediction systems agree fairly well with each other, although the isopleths predicted by the ERSM technique are not as smooth as those predicted by the conventional RSM technique owing to a much larger variable number. The consistency between the conventional RSM and ERSM prediction systems indicates that the ERSM technique could reproduce fairly well the response of $PM_{2.5}$ to continuous changes of precursor emission levels between zero and 150 %. Although model simulations definitely have numerical errors, the success in capturing the atmospheric responses to continuous emission changes over a full range of control levels ensures that these errors could not challenge the major conclusions about the effectiveness of air pollution control measures.

GMDD
7, 5049–5085, 2014

3.2 Response of $PM_{2.5}$ to precursor emissions

The ERSM prediction system could instantly evaluate the response of $PM_{2.5}$ and its chemical components to the independent or simultaneous changes of the precursor emissions from multiple sectors and regions, over a full range of control levels. Therefore, it improves the identification of major precursors, regions, and sectors contributing to $PM_{2.5}$ pollution. This unique capability distinguishes the ERSM from the previous sensitivity analysis methods.

Following previous sensitivity studies, we define $PM_{2.5}$ sensitivity as the change ratio of $PM_{2.5}$ concentration divided by the reduction ratio of emissions:

$$S_a^X = \left[(C^* - C_a)/C^*\right]/(1-a) \quad (18)$$

where S_a^X is the $PM_{2.5}$ sensitivity to emission source X at its emission ratio a; C_a is the concentration of $PM_{2.5}$ when the emission ratio of X is a; and C^* is the concentration of $PM_{2.5}$ in the base case (when emission ratio of X is 1). Figure 6 shows the $PM_{2.5}$ sensitivity to the stepped control of individual air pollutants, and Fig. 7 shows the $PM_{2.5}$ sensitivity to the stepped control of individual air pollutants from individual sectors. Figure 6 can be derived from the prediction systems built with both the conventional RSM and ERSM technique, except that the latter did not evaluate the effects of the changes of NMVOC emissions. The results derived from both systems are consistent, and we present those derived from the conventional technique to include the effects of NMVOC. Figure 7 is derived from the ERSM technique.

In January, $PM_{2.5}$ concentrations are sensitive to the primary $PM_{2.5}$ emissions, followed by NH_3, and relatively insensitive to NO_X and SO_2. The contribution of primary $PM_{2.5}$ is dominated by the emissions from industrial and residential sources. During August, gaseous precursors make larger contributions to $PM_{2.5}$ concentrations than primary $PM_{2.5}$, with similar contributions from NH_3, SO_2, and NO_X. The NO_X emissions from power plants, the industrial and residential sector, and the transportation sector play similar roles; the SO_2 emissions from the industrial and residential sector

GMDD
7, 5049–5085, 2014

have larger effects on $PM_{2.5}$ than those from power plants due to larger emissions and lower stack heights. NMVOC emissions have minor effect on $PM_{2.5}$ concentrations, mainly due to the significant underestimation of SOA in the current version of CMAQ, which is also a common issue for most widely used air quality models (Robinson et al., 2007).

The $PM_{2.5}$ sensitivities to primary $PM_{2.5}$ emissions are approximately the same at various control levels. However, the $PM_{2.5}$ sensitivity to gaseous precursors increases notably when more control efforts are taken, mainly attributable to transition between NH_3-rich and NH_3-poor conditions. Specifically, a particular pollutant (SO_2, NO_X, or NH_3), when subject to larger reductions compared with others, will become the limiting factor for inorganic aerosol chemistry. In January, the response of $PM_{2.5}$ to NO_X emissions is negative for relatively small reductions (< 40–70 %), but becomes positive for large reductions (> 40–70 %). This strong nonlinearity has also been confirmed by the previous studies (Zhao et al., 2013c; Dong et al., 2014). Relatively small reductions of NO_X emissions lead to the increase of O_3 and HO_X radical due to a NMVOC-limited regime for photochemistry, enhancing the formation of sulfate (see Fig. 8). In addition, the increase of O_3 and HO_X radical also accelerates the nighttime formation of N_2O_5 and HNO_3 through the $NO_2 + O_3$ reaction, thereby enhancing the formation of nitrate aerosol (see Fig. 8). As an integrated effect, the $PM_{2.5}$ concentrations increase with relatively small reductions of NO_X emissions. Under large reductions of NO_X, $PM_{2.5}$ concentrations decrease, resulting from the simultaneous decline of NO_2, O_3 and HO_X radical concentrations (NO_X-limited regime for photochemistry). These chemical processes also explain why the reduction of NO_X emissions of a single economic sector has negative effects on $PM_{2.5}$ even at large reduction ratio (see Fig. 7). Simultaneous reductions of NO_X emissions from multiple sectors are essential for reducing $PM_{2.5}$ concentrations. If all pollutants are controlled simultaneously, the sensitivity of $PM_{2.5}$ concentrations to emission reductions also generally becomes larger with more control effort taken, especially in January (see red dotted line in Fig. 6).

GMDD
7, 5049–5085, 2014

Then, we evaluate the contribution of primary $PM_{2.5}$ and gaseous precursor (SO_2, NO_X, and NH_3) emissions from different regions to $PM_{2.5}$ concentrations based on the ERSM technique (Table 3). The contributions of total primary $PM_{2.5}$ emissions (39–46 % in January, and 43–46 % in August) are dominated by local sources (32–36 % in January, and 37–43 % in August). Total gaseous precursor emissions in the domain contribute 25–36 % and 48–50 % of $PM_{2.5}$ concentrations in January and August, respectively. The relative importance of gaseous precursor emissions from the other regions compared with local precursor emissions is generally higher than that of primary $PM_{2.5}$; this trend is especially evident in August. In Shanghai, the gaseous precursor emissions from Jiangsu and Zhejiang even contribute more to the $PM_{2.5}$ concentration than local precursor emissions during August. In January, long range transport has a significant effect on $PM_{2.5}$ concentrations (25–34 % contribution) due to the northerly monsoon, contrasted by the minor effect in August (7–8 % contribution).

3.3 Response of SO_4^{2-} and NO_3^- to precursor emissions

We pay special attention to secondary inorganic aerosols (SIA) because SIA contribute 28–55 % of total $PM_{2.5}$ concentrations based on our simulation. Figure 8 shows the sensitivity of NO_3^-/SO_4^{2-} concentrations to the emissions of individual air pollutants in individual regions; Fig. S4 shows the sensitivity of NO_3^-/SO_4^{2-} concentrations to the emissions of individual air pollutants from individual sectors. Both figures are derived from the prediction system built with the ERSM technique. In January, NO_3^- concentration is most sensitive to NH_3 emissions, especially local NH_3 emissions. The effect of local NO_X emissions on NO_3^- concentrations changes from negative to positive when the controls of NO_X emissions become more and more stringent. This pattern is similar to that of $PM_{2.5}$ described above. The NO_X emissions from the industrial and residential sector and the transportation sector, when controlled individually, both make negative contribution to the reduction of NO_3^- concentrations. In contrast, the control of NO_X emissions from power plants often favors the reduction of NO_3^-, because power

GMDD
7, 5049–5085, 2014

plants tend to affect the fine particles over a larger spatial scale due to their higher release heights, and because the photochemistry typically changes from a NMVOC-limited regime in surface metropolis areas to a NO_X-limited regime in vast rural areas or the upper air (Xing et al., 2011). In August, NO_3^- concentrations are mainly affected by local emissions of NH_3 and NO_X, as well as NO_X emissions in upwind regions, and NO_X emissions make a much larger positive contribution to NO_3^- concentrations compared with January. Factors accounting for this difference include a stronger NH_3-rich condition for inorganic aerosol chemistry (Wang et al., 2011), and a weaker NMVOC-limited (in metropolis areas) or a stronger NO_X-limited (in rural areas) photochemical condition in August. The contributions of NO_X emissions from power plants, the industrial and residential sector, and the transportation sector are similar to each other.

In January, SO_4^{2-} concentrations are dominated by the changes of local SO_2 emissions, followed by local NH_3 emissions. NO_X emissions have a negative effect on SO_4^{2-} due to both thermodynamic (competition with SO_2 for NH_3) and photochemical effect (negatively correlated with O_3 and HO_X radical). In August, SO_4^{2-} is most sensitive to local SO_2 and NH_3 emissions. In Shanghai, where local emissions are relatively small compared with emissions in other regions, the SO_2 and NH_3 emissions from upwind regions might contribute more to SO_4^{2-} concentration than local emissions. In both January and August, the SO_2 emissions of the industrial and residential sector have larger effects on SO_4^{2-} concentrations than those of power plants, partly due to larger emissions and lower stack heights.

4 Conclusions and implications

In this study, we developed a novel Extended Response Surface Modeling technique (ERSM v1.0). As an advantage over previous models or techniques, this technique could characterize the nonlinear response of $PM_{2.5}$ and its chemical components to large and simultaneous changes of multiple precursor emissions from multiple regions

GMDD
7, 5049–5085, 2014

and sectors with a reasonable number of model scenarios. The ERSM technique was developed starting from the conventional RSM technique; it first quantifies the relationship between $PM_{2.5}$ concentrations and precursor emissions in a single region with the conventional RSM technique, and then assesses the effects of inter-regional transport of $PM_{2.5}$ and its precursors on $PM_{2.5}$ concentrations in the target region. A particular algorithm was implemented to improve the accuracy of the response surface when the emissions from multiple regions experience quite large reductions simultaneously.

We applied the ERSM technique with CMAQ version 4.7.1 over the YRD region of China, and mapped the concentrations of $PM_{2.5}$ and its inorganic componets vs. 36 control variables. Using the ERSM technique, we predicted the $PM_{2.5}$ concentrations for 40 independent control scenarios, and compared with the corresponding CMAQ simulations. The comparison results show that the ERSM predictions and CMAQ simulations agree well with each other. The correlation coefficients are larger than 0.98 and 0.99, and the mean normalized errors are less than 1 and 2 % for January and August, respectively. We also compared the 2-D-isopleths of $PM_{2.5}$ concentrations in response to the changes of precursor emissions derived from both the conventional RSM and the ERSM technique, and demonstrated that the ERSM technique could reproduce fairly well the response of $PM_{2.5}$ to continuous changes of precursor emission levels between zero and 150 %.

Employing the ERSM technique, we identified the major sources contributing to $PM_{2.5}$ and its inorganic components in the YRD region. For example, in January, $PM_{2.5}$ concentrations are sensitive to the primary $PM_{2.5}$ emissions, followed by NH_3, and relatively insensitive to NO_X and SO_2. During August, gaseous precursors make larger contributions to $PM_{2.5}$ concentrations than primary $PM_{2.5}$, with similar contributions from NH_3, SO_2, and NO_X. We also characterized the nonlinearity in the response of $PM_{2.5}$ to emission changes and illustrated the underlying chemical processes. For example, the sensitivity of $PM_{2.5}$ to gaseous precursors increases notably when more control efforts are taken, due to the transition between NH_3-rich and NH_3-poor conditions. In January,

GMDD
7, 5049–5085, 2014

the response of $PM_{2.5}$ to NO_X emissions is negative for relatively small reductions, but becomes positive for large reductions.

The assessment of the response of $PM_{2.5}$ and its inorganic components to precursor emissions over the YRD region has important policy implications. First, the control of primary $PM_{2.5}$ emissions, especially those of the industrial and residential sources, should be enhanced considering their large contribution to $PM_{2.5}$ concentrations. Second, NO_X emissions need be reduced substantially in order to mitigate the adverse effect on $PM_{2.5}$ concentrations at relatively small reduction ratio. Third, the control of NH_3 should be implemented in heavy-pollution areas in winter due to its significant effect on $PM_{2.5}$. Fourth, it is essential to implement region-dependent emission reduction targets based on the above-quantified interactions among regions.

Except for identification of major emission sources, the ERSM technique has several other practical applications. First, it allows us to calculate the required emission reductions to attain a certain environmental target. Specifically, we alter the emission ratios of various control variables and calculate the "real-time" response of $PM_{2.5}$ concentrations with ERSM repeatedly until the standard is attained. Second, ERSM can be applied to design optimal control options, which could be determined through cost-effective optimization once ERSM is coupled with control cost models/functions that links the emission reductions with private costs.

Code availability

All codes needed to run ERSM v1.0 in MATLAB® are available upon the request. Any potential user interested in the model should contact S. X. Wang, and any feedback on them is welcome. Procedures to run the model and sources of external data files are properly documented in a Manual.doc file.

GMDD
7, 5049–5085, 2014

Author contribution

B. Zhao, J. Xing, and S. X. Wang developed the underlying algorithms of the model. B. Zhao and K. Fu developed the model code and performed the simulations. B. Zhao, K. Fu and W. J. Wu conducted the model validation. B. Zhao and S. X. Wang prepared the manuscript with contributions from all co-authors. J. S. Fu, C. Jang, Y. Zhu, X. Y. Dong, Y. Gao and J. M. Hao provided important acadamic guidance.

The Supplement related to this article is available online at doi:10.5194/gmdd-7-5049-2014-supplement.

Acknowledgements. This work was sponsored by National Natural Science Foundation of China (21221004), Strategic Priority Research Program of the Chinese Academy of Sciences (XBD05020300), and special fund of State Key Joint Laboratory of Environment Simulation and Pollution Control (12L05ESPC). The corresponding author, Shuxiao Wang, is supported by the Program for New Century Excellent Talents in University (NCET-10-0532) and the China Scholarship Council. The authors also appreciate the support from Collaborative Innovation Center for Regional Environmental Quality of Tsinghua University.

References

Amann, M., Cofala, J., Gzella, A., Heyes, C., Klimont, Z., and Schopp, W.: Estimating Concentrations of Fine Particulate Matter in Urban Background Air of European Cities, Interim Report IR-07-001, available at: http://www.iiasa.ac.at (last access: 30 July 2014), International Institute for Applied Systems Analysis, Laxenburg, Austria, 50, 2007.

Carlton, A. G., Bhave, P. V., Napelenok, S. L., Edney, E. D., Sarwar, G., Pinder, R. W., Pouliot, G. A., and Houyoux, M.: Model representation of secondary organic aerosol in CMAQv4.7, Environ. Sci. Technol., 44, 8553–8560, doi:10.1021/Es100636q, 2010.

GMDD

7, 5049–5085, 2014

Carmichael, G. R., Sandu, A., and Potra, F. A.: Sensitivity analysis for atmospheric chemistry models via automatic differentiation, Atmos. Environ., 31, 475–489, doi:10.1016/S1352-2310(96)00168-9, 1997.

Carnevale, C., Finzi, G., Pisoni, E., and Volta, M.: Neuro-fuzzy and neural network systems for air quality control, Atmos. Environ., 43, 4811–4821, doi:10.1016/j.atmosenv.2008.07.064, 2009.

Dickerson, R. R., Stedman, D. H., and Delany, A. C.: Direct measurements of ozone and nitrogen-dioxide photolysis rates in the troposphere, J. Geophys. Res.-Oc. Atm., 87, 4933–4946, doi:10.1029/Jc087ic07p04933, 1982.

Dong, X. Y., Li, J., Fu, J. S., Gao, Y., Huang, K., and Zhuang, G. S.: Inorganic aerosols responses to emission changes in Yangtze River Delta, China, Sci. Total. Environ., 481, 522–532, doi:10.1016/j.scitotenv.2014.02.076, 2014.

Fu, J. S., Brill, E. D., and Ranjithan, S. R.: Conjunctive use of models to design cost-effective ozone control strategies, J. Air. Waste. Manage., 56, 800–809, 2006.

Fu, X., Wang, S. X., Zhao, B., Xing, J., Cheng, Z., Liu, H., and Hao, J. M.: Emission inventory of primary pollutants and chemical speciation in 2010 for the Yangtze River Delta region, China, Atmos. Environ., 70, 39–50, doi:10.1016/j.atmosenv.2012.12.034, 2013.

Guenther, A., Karl, T., Harley, P., Wiedinmyer, C., Palmer, P. I., and Geron, C.: Estimates of global terrestrial isoprene emissions using MEGAN (Model of Emissions of Gases and Aerosols from Nature), Atmos. Chem. Phys., 6, 3181–3210, doi:10.5194/acp-6-3181-2006, 2006.

Hakami, A., Odman, M. T., and Russell, A. G.: High-order, direct sensitivity analysis of multidimensional air quality models, Environ. Sci. Technol., 37, 2442–2452, doi:10.1021/Es020677h, 2003.

Hakami, A., Seinfeld, J. H., Chai, T. F., Tang, Y. H., Carmichael, G. R., and Sandu, A.: Adjoint sensitivity analysis of ozone nonattainment over the continental United States, Environ. Sci. Technol., 40, 3855–3864, doi:10.1021/Es052135g, 2006.

Heyes, C., Schopp, W., Amann, M., and Unger, S.: A Reduced-Form Model to Predict Long-Term Ozone Concentrations in Europe, Interim Report WP-96-12, available at: http://www.iiasa.ac.at (last access: 30 July 2014), International Institute for Applied Systems Analysis, Laxenburg, Austria, 58, 1996.

Hwang, J. T., Dougherty, E. P., Rabitz, S., and Rabitz, H.: Greens function method of sensitivity analysis in chemical-kinetics, J. Chem. Phys., 69, 5180–5191, doi:10.1063/1.436465, 1978.

GMDD
7, 5049–5085, 2014

Iman, R. L., Davenport, J. M., and Zeigler, D. K.: Latin Hypercube Sampling (Program User's Guide), US Technical Report SAND79-1473, Sandia National Laboratories, Albuquerque, NM, 78, 1980.

Milford, J. B., Russell, A. G., and Mcrae, G. J.: A new approach to photochemical pollution-control – implications of spatial patterns in pollutant responses to reductions in nitrogen-oxides and reactive organic gas emissions, Environ. Sci. Technol., 23, 1290–1301, doi:10.1021/Es00068a017, 1989.

Nel, A.: Air pollution-related illness: effects of particles, Science, 308, 804–806, doi:10.1126/science.1108752, 2005.

Robinson, A. L., Donahue, N. M., Shrivastava, M. K., Weitkamp, E. A., Sage, A. M., Grieshop, A. P., Lane, T. E., Pierce, J. R., and Pandis, S. N.: Rethinking organic aerosols: semivolatile emissions and photochemical aging, Science, 315, 1259–1262, doi:10.1126/science.1133061, 2007.

Russell, A., Milford, J., Bergin, M. S., Mcbride, S., Mcnair, L., Yang, Y., Stockwell, W. R., and Croes, B.: Urban ozone control and atmospheric reactivity of organic gases, Science, 269, 491–495, doi:10.1126/science.269.5223.491, 1995.

Sandu, A. and Zhang, L.: Discrete second order adjoints in atmospheric chemical transport modeling, J. Comput. Phys., 227, 5949–5983, doi:10.1016/j.jcp.2008.02.011, 2008.

Sandu, A., Daescu, D. N., Carmichael, G. R., and Chai, T. F.: Adjoint sensitivity analysis of regional air quality models, J. Comput. Phys., 204, 222–252, doi:10.1016/j.jcp.2004.10.011, 2005.

Santner, T. J., Williams, B. J., and Notz, W.: The Design and Analysis of Computer Experiments, Springer Verlag, New York, US, 283 pp., 2003.

Simon, H., Baker, K. R., Akhtar, F., Napelenok, S. L., Possiel, N., Wells, B., and Timin, B.: A direct sensitivity approach to predict hourly ozone resulting from compliance with the national ambient air quality standard, Environ. Sci. Technol., 47, 2304–2313, doi:10.1021/Es303674e, 2013.

Stocker, T. F., Qin, D., Plattner, G.-K., Tignor, M., Allen, S. K., Boschung, J., Nauels, A., Xia, Y., Bex, V., and Midgley, P. M.: Climate Change 2013: The Physical Science Basis. Contribution of Working Group I to the Fifth Assessment Report of the Intergovernmental Panel on Climate Change, Cambridge University Press, Cambridge, UK and New York, NY, USA, 1535 pp., 2013.

GMDD
7, 5049–5085, 2014

US Environmental Protection Agency: Technical Support Document for the Proposed PM NAAQS Rule: Response Surface Modeling, Office of Air Quality Planning and Standards, US Environmental Protection Agency, Research Triangle Park, NC, US, 48, 2006a.
US Environmental Protection Agency: Technical Support Document for the Proposed Mobile Source Air Toxics Rule: Ozone Modeling, Office of Air Quality Planning and Standards, US Environmental Protection Agency, Research Triangle Park, NC, US, 49, 2006b.
Wang, L. H. and Milford, J. B.: Reliability of optimal control strategies for photochemical air pollution, Environ. Sci. Technol., 35, 1173–1180, doi:10.1021/Es001358y, 2001.
Wang, S. X. and Hao, J. M.: Air quality management in China: issues, challenges, and options, J. Environ. Sci-China, 24, 2–13, doi:10.1016/S1001-0742(11)60724-9, 2012.
Wang, S. X., Xing, J., Jang, C. R., Zhu, Y., Fu, J. S., and Hao, J. M.: Impact assessment of ammonia emissions on inorganic aerosols in east China using response surface modeling technique, Environ. Sci. Technol., 45, 9293–9300, doi:10.1021/Es2022347, 2011.
Wang, S. X., Zhao, B., Cai, S. Y., Klimont, Z., Nielsen, C. P., Morikawa, T., Woo, J. H., Kim, Y., Fu, X., Xu, J. Y., Hao, J. M., and He, K. B.: Emission trends and mitigation options for air pollutants in East Asia, Atmos. Chem. Phys., 14, 6571–6603, doi:10.5194/acp-14-6571-2014, 2014.
Xing, J.: Study on the Nonlinear Responses of Air Quality to Primary Pollutant Emissions, Doctor thesis, School of Environment, Tsinghua University, Beijing, China, 138 pp., 2011 (in Chinese).
Xing, J., Wang, S. X., Jang, C., Zhu, Y., and Hao, J. M.: Nonlinear response of ozone to precursor emission changes in China: a modeling study using response surface methodology, Atmos. Chem. Phys., 11, 5027–5044, doi:10.5194/acp-11-5027-2011, 2011.
Yang, Y. J., Wilkinson, J. G., and Russell, A. G.: Fast, direct sensitivity analysis of multidimensional photochemical models, Environ. Sci. Technol., 31, 2859–2868, doi:10.1021/Es970117w, 1997.
Yarwood, G., Emery, C., Jung, J., Nopmongcol, U., and Sakulyanontvittaya, T.: A method to represent ozone response to large changes in precursor emissions using high-order sensitivity analysis in photochemical models, Geosci. Model Dev., 6, 1601–1608, doi:10.5194/gmd-6-1601-2013, 2013.
Zhang, Q., Streets, D. G., Carmichael, G. R., He, K. B., Huo, H., Kannari, A., Klimont, Z., Park, I. S., Reddy, S., Fu, J. S., Chen, D., Duan, L., Lei, Y., Wang, L. T., and Yao, Z. L.: Asian

GMDD
7, 5049–5085, 2014

emissions in 2006 for the NASA INTEX-B mission, Atmos. Chem. Phys., 9, 5131–5153, doi:10.5194/acp-9-5131-2009, 2009.

Zhang, X. Y., Wang, Y. Q., Niu, T., Zhang, X. C., Gong, S. L., Zhang, Y. M., and Sun, J. Y.: Atmospheric aerosol compositions in China: spatial/temporal variability, chemical signature, regional haze distribution and comparisons with global aerosols, Atmos. Chem. Phys., 12, 779–799, doi:10.5194/acp-12-779-2012, 2012.

Zhang, Y., Wen, X. Y., Wang, K., Vijayaraghavan, K., and Jacobson, M. Z.: Probing into regional O_3 and particulate matter pollution in the United States: 2. An examination of formation mechanisms through a process analysis technique and sensitivity study, J. Geophys. Res.-Atmos., 114, D22305, doi:10.1029/2009jd011900, 2009.

Zhao, B., Wang, S. X., Dong, X. Y., Wang, J. D., Duan, L., Fu, X., Hao, J. M., and Fu, J.: Environmental effects of the recent emission changes in China: implications for particulate matter pollution and soil acidification, Environ. Res. Lett., 8, 024031, doi:10.1088/1748-9326/8/2/024031, 2013a.

Zhao, B., Wang, S. X., Liu, H., Xu, J. Y., Fu, K., Klimont, Z., Hao, J. M., He, K. B., Cofala, J., and Amann, M.: NO_x emissions in China: historical trends and future perspectives, Atmos. Chem. Phys., 13, 9869–9897, doi:10.5194/acp-13-9869-2013, 2013b.

Zhao, B., Wang, S. X., Wang, J. D., Fu, J. S., Liu, T. H., Xu, J. Y., Fu, X., and Hao, J. M.: Impact of national NO_x and SO_2 control policies on particulate matter pollution in China, Atmos. Environ., 77, 453–463, doi:10.1016/j.atmosenv.2013.05.012, 2013c.

GMDD
7, 5049–5085, 2014

Table 1. Description of the RSM/ERSM prediction systems developed in this study.

method	variable number	control variables	scenario number	scenario details
conventional RSM technique	5	total emissions of NO_X, SO_2, NH_3, NMVOC, and $PM_{2.5}$	101	1 CMAQ base case; 100[a] scenarios generated by applying LHS method for the 5 variables.
ERSM technique	36	9 variables in each of the 4 regions, including 6 gaseous variables, i.e., (1) NO_X/Power plants (2) NO_X/Industrial and residential (3) NO_X/Transportation (4) SO_2/Power plants (5) SO_2/Industrial and Residential (6) NH_3/All sectors, and 3 primary $PM_{2.5}$ variables, i.e., (7) $PM_{2.5}$/Power plants (8) $PM_{2.5}$/Industrial and residential (9) $PM_{2.5}$/Transportation.	663	1 CMAQ base case; 600 scenarios, including 150[a] scenarios generated by applying LHS method for the gaseous control variables in Shanghai, 150 scenarios generated in the same way for Jiangsu, 150 scenarios for Zhejiang, 150 scenarios for Others; 50[a] scenarios generated by applying LHS method for the total NO_X, SO_2, and NH_3 emissions; 12 scenarios where one primary $PM_{2.5}$ control variable is set to 0.25 for each scenario.

[a] 100, 150 and 50 scenarios are needed for the response surfaces for 5, 6 and 3 variables, respectively (Xing et al., 2011; Wang et al., 2011).

GMDD
7, 5049–5085, 2014

Table 2. Comparison of $PM_{2.5}$ concentrations predicted by the ERSM technique with out-of-sample CMAQ simulations.

	January			August		
	Shanghai	Jiangsu	Zhejiang	Shanghai	Jiangsu	Zhejiang
Correlation coefficient	0.989	0.980	0.987	0.995	0.997	0.994
Mean Normalized Error (MNE)	1.0 %	0.7 %	0.9 %	0.8 %	0.5 %	1.7 %
Maximum Normalized Error (NE)	4.5 %	3.0 %	5.2 %	10.2 %	7.7 %	9.6 %
95 % percentile of NEs	2.8 %	2.7 %	3.5 %	3.0 %	1.6 %	3.1 %
MNE (case 33–36)	0.0 %	0.0 %	0.0 %	0.1 %	0.1 %	0.1 %
Maximum NE (case 33–36)	0.1 %	0.1 %	0.1 %	0.1 %	0.1 %	0.2 %

GMDD
7, 5049–5085, 2014

Table 3. Contribution of primary $PM_{2.5}$ and gaseous precursor (NO_X, SO_2, NH_3) emissions from individual regions to $PM_{2.5}$ concentrations.

	January Shanghai	Jiangsu	Zhejiang	August Shanghai	Jiangsu	Zhejiang
Emissions of Primary $PM_{2.5}$ in Shanghai	35.5 %	1.1 %	1.3 %	36.9 %	1.0 %	0.4 %
Emissions of Primary $PM_{2.5}$ in Jiangsu	5.6 %	35.0 %	4.1 %	2.2 %	37.5 %	0.9 %
Emissions of Primary $PM_{2.5}$ in Zhejiang	1.9 %	2.3 %	32.2 %	4.3 %	2.5 %	42.8 %
Emissions of Primary $PM_{2.5}$ in Others	2.9 %	2.9 %	1.7 %	2.0 %	1.9 %	1.5 %
Emissions of Primary $PM_{2.5}$ in four regions	46.0 %	41.2 %	39.4 %	45.4 %	42.9 %	45.7 %
Emissions of NO_X, SO_2, and NH_3 in Shanghai	11.3 %	0.2 %	1.0 %	18.9 %	1.8 %	2.5 %
Emissions of NO_X, SO_2, and NH_3 in Jiangsu	3.3 %	11.7 %	3.9 %	5.2 %	30.1 %	4.3 %
Emissions of NO_X, SO_2, and NH_3 in Zhejiang	2.7 %	4.3 %	20.9 %	18.3 %	12.6 %	36.3 %
Emissions of NO_X, SO_2, and NH_3 in Others	1.7 %	2.4 %	2.8 %	5.7 %	4.6 %	7.2 %
Emissions of NO_X, SO_2, and NH_3 in four regions	25.2 %	24.9 %	35.7 %	48.3 %	50.4 %	47.7 %
Emissions of Primary $PM_{2.5}$ in the outer domain	7.4 %	9.1 %	6.3 %	0.7 %	0.8 %	1.6 %
Emissions of NO_X, SO_2, and NH_3 in outer domain	20.6 %	24.5 %	19.1 %	6.6 %	7.1 %	6.1 %

GMDD
7, 5049–5085, 2014

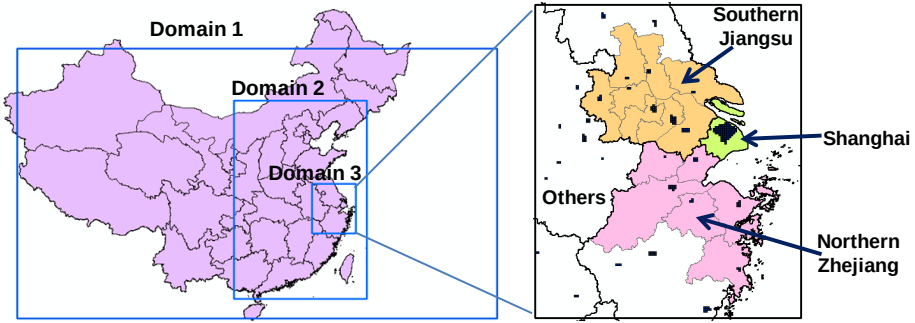

Figure 1. Triple nesting domains used in CMAQ simulation (left) and the definition of four regions in the innermost domain, denoted by different colors (right). The black lines in the left figure represent provincial boundaries; the thick black lines and the thin grey lines in the right figure represent the provincial boundaries and city boundaries, respectively. The dark blue grids in the right figure represent the urban areas of major cities.

GMDD
7, 5049–5085, 2014

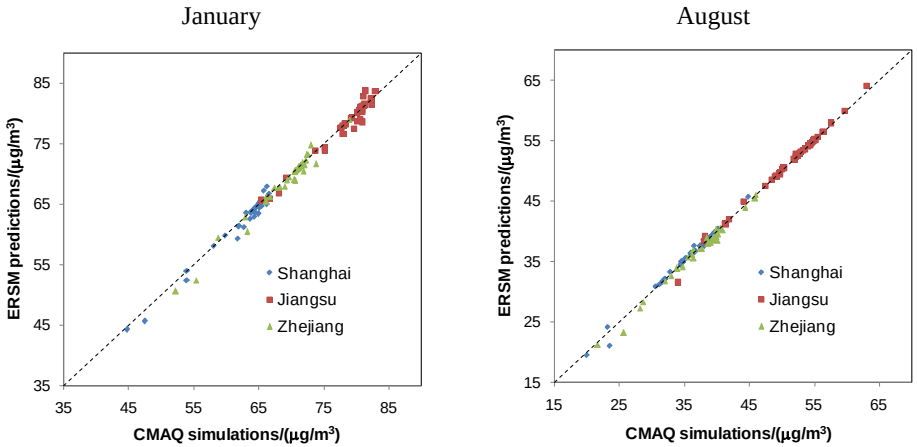

Figure 2. Comparison of $PM_{2.5}$ concentrations predicted by the ERSM technique with out-of-sample CMAQ simulations. The dashed line is the one-to-one line indicating perfect agreement.

GMDD
7, 5049–5085, 2014

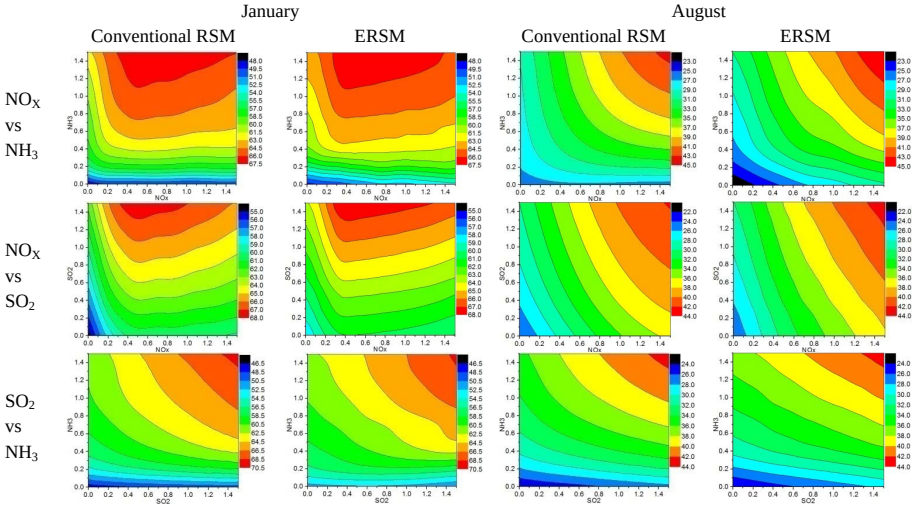

Figure 3. Comparison of the 2-D isopleths of $PM_{2.5}$ concentrations in Shanghai in response to precursor emissions derived from the conventional RSM technique and the ERSM technique in Shanghai. The *X* and *Y* axis shows the emission ratio, defined as the ratios of the changed emissions to the emissions in the base case. The different colors represent different $PM_{2.5}$ concentrations.

GMDD
7, 5049–5085, 2014

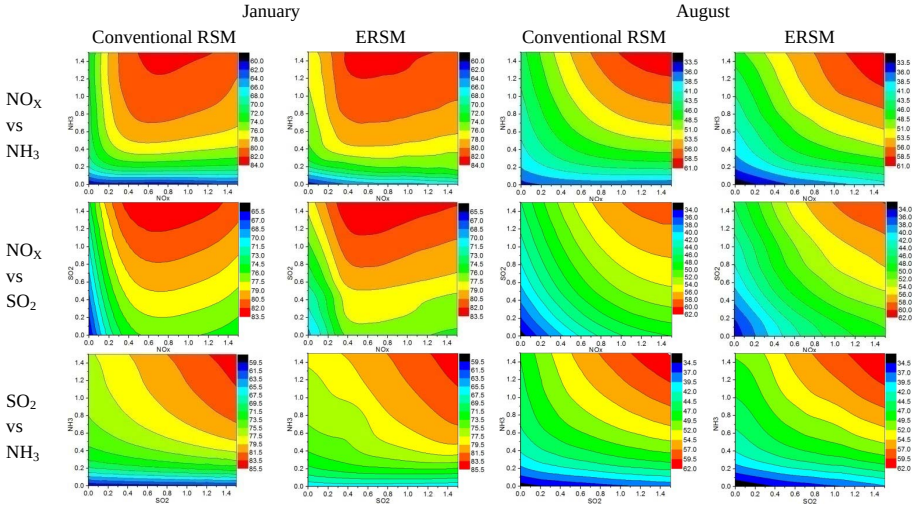

Figure 4. The same as Fig. 3 but for the region of Jiangsu.

GMDD
7, 5049–5085, 2014

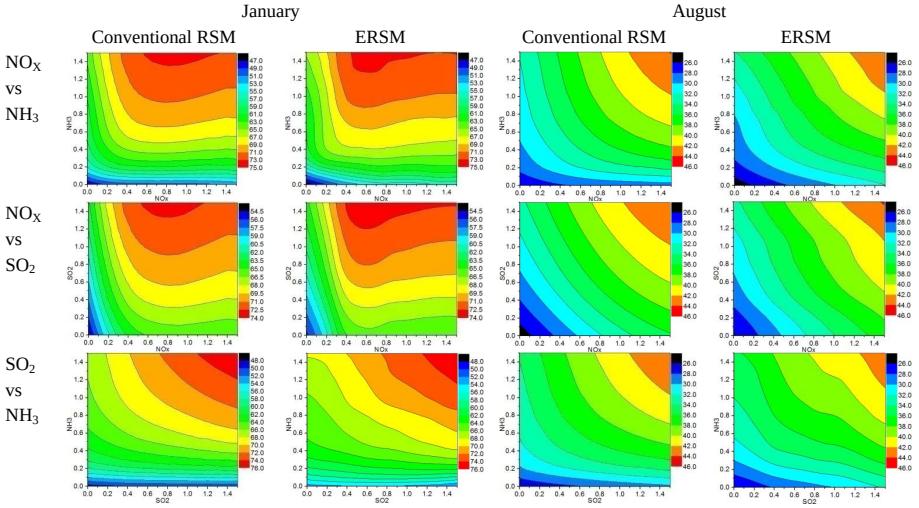

Figure 5. The same as Fig. 3 but for the region of Zhejiang.

GMDD
7, 5049–5085, 2014

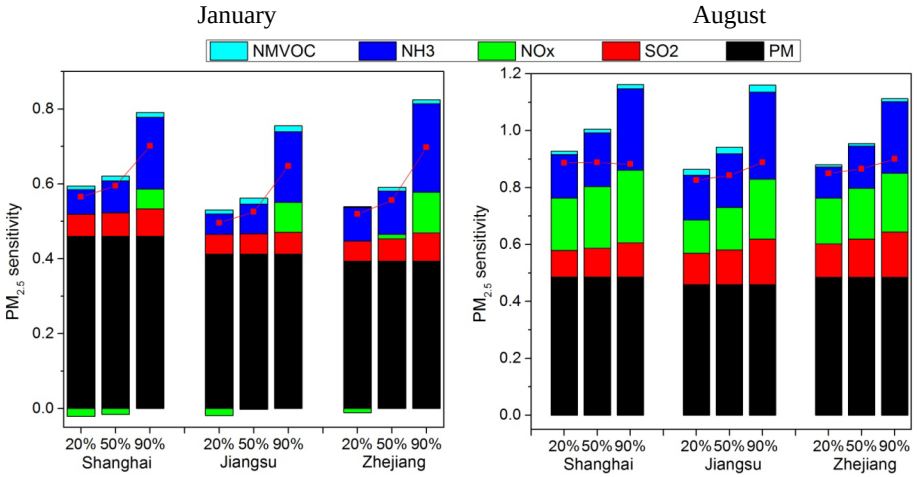

Figure 6. Sensitivity of $PM_{2.5}$ concentrations to the stepped control of individual air pollutants. The *X* axis shows the reduction ratio (= 1 – emission ratio). The *Y* axis shows $PM_{2.5}$ sensitivity, which is defined as the change ratio of concentration divided by the reduction ratio of emissions. The colored bars denote the $PM_{2.5}$ sensitivities when a particular pollutant is controlled while the others stay the same as the base case; the red dotted line denotes the $PM_{2.5}$ sensitivity when all emission sources are controlled simultaneously.

GMDD
7, 5049–5085, 2014

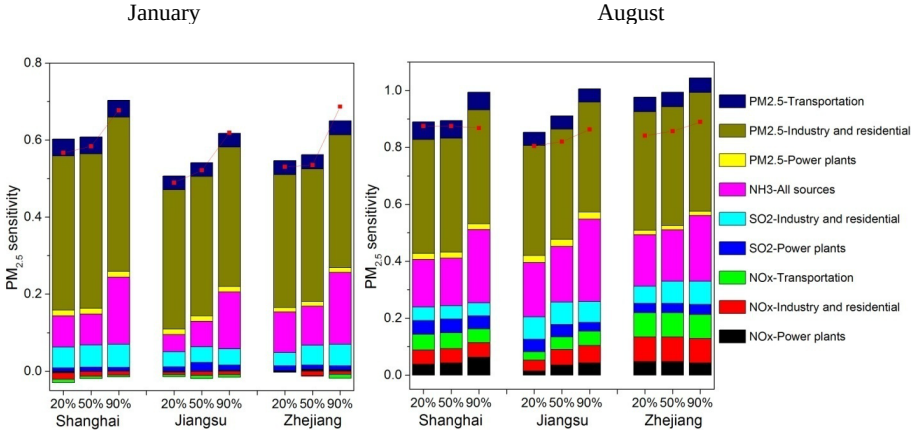

Figure 7. Sensitivity of $PM_{2.5}$ concentrations to the stepped control of individual air pollutants from individual sectors. The *X* axis shows the reduction ratio (= 1 – emission ratio). The *Y* axis shows $PM_{2.5}$ sensitivity, which is defined as the change ratio of concentration divided by the reduction ratio of emissions. The colored bars denote the $PM_{2.5}$ sensitivities when a particular emission source is controlled while the others stay the same as the base case; the red dotted line denotes the $PM_{2.5}$ sensitivity when all emission sources are controlled simultaneously.

GMDD
7, 5049–5085, 2014

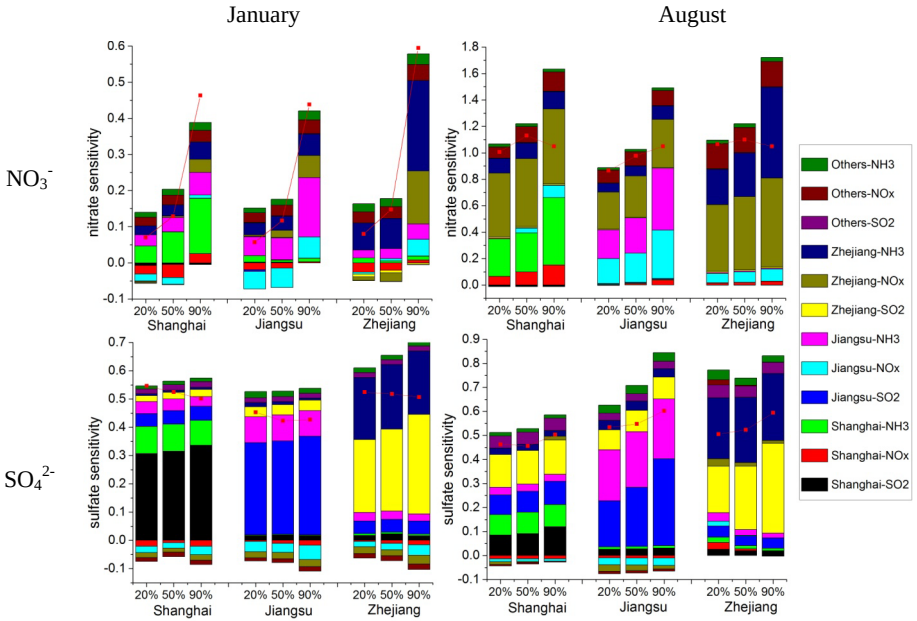

Figure 8. Sensitivity of NO_3^- and SO_4^{2-} concentrations to the stepped control of individual air pollutants in individual regions. The *X* axis shows the reduction ratio (= 1 – emission ratio). The *Y* axis shows NO_3^-/SO_4^{2-} sensitivity, which is defined as the change ratio of NO_3^-/SO_4^{2-} concentration divided by the reduction ratio of emissions. The colored bars denote the NO_3^-/SO_4^{2-} sensitivities when a particular emission source is controlled while the others stay the same as the base case; the red dotted line denotes the NO_3^-/SO_4^{2-} sensitivity when all emission sources are controlled simultaneously.

GMDD
7, 5049–5085, 2014